Journal of Mineralogical and Petrological Sciences (2026) 121:002

New epidote-supergroup minerals from the Mogurazawa mine, Gunma, Japan: akasakaite-(Ce), akasakaite-(La), vanadoakasakaite-(Ce), and vanadoakasakaite-(La)

Mariko NAGASHIMA*, Daisuke NISHIO-HAMANE**, Masayuki OHNISHI***, Hiroshi MIYAJIMA† and Akira HARADA‡

*Division of Earth Science, Graduate School of Science and Technology for Innovation, Yamaguchi University, Yamaguchi 753-8512, Japan
**The Institute for Solid State Physics, the University of Tokyo, Kashiwa 277-8581, Japan
***Takehana Ougi-cho, Yamashina-ku, Kyoto 607-8082, Japan
†Nozawa, Saku, Nagano 385-0053, Japan
‡Midorigaoka, Chuo-ku, Sagamihara, Kanagawa 252-0225, Japan

New allanite-group minerals, akasakaite-(Ce), akasakaite-(La), vanadoakasakaite-(Ce), and vanadoakasakaite-(La), associated with small quartz lenses within rhodonite-enriched rocks of the stratiform manganese deposits at the Mogurazawa mine, Gunma, Japan, were studied using electron microprobe analysis, Raman spectroscopy, and single-crystal X-ray diffraction methods. Akasakaite is defined by the ideal formula, $^{A1}Ca^{A2}REE^{3+M1}Me^{3+}{}^{M2}Al^{M3}Mn^{2+}(SiO_4)(Si_2O_7)O(OH)$ (Z = 2, space group $P2_1/m$). The four new minerals are distinguished by the dominant cation at the $M1$ site (Al or V^{3+}) and the dominant REE^{3+} at the $A2$ site (Ce or La). The unit-cell parameters are a = 8.885-8.925, b = 5.694-5.744, c = 10.100-10.153 Å, β = 113.62-113.79°, and V = 468.0-476.4 Å^3. Structure refinements converged to $R1$ values of 2.20-2.86%. At the $M1$ site, Al content reaches 85% in akasakaite-(La), whereas V^{3+} reaches 82% in vanadoakasakaite-(La). The cation assignments for these specimens are as follows: $^{A1}Ca_{0.54}Mn^{2+}_{0.46}$, $^{A2}La_{0.53}Ce_{0.18}Nd_{0.05}Pr_{0.02}Sr_{0.04}Ca_{0.18}$, $^{M1}Al_{0.85}V^{3+}_{0.13}Ti_{0.02}$, $^{M2}Al_{1.00}$, and $^{M3}Mn^{2+}_{0.75}Fe_{0.01}V^{3+}_{0.16}Al_{0.07}$ for akasakaite-(La) and $^{A1}Ca_{0.60}Mn^{2+}_{0.40}$, $^{A2}La_{0.45}Ce_{0.17}Nd_{0.06}Pr_{0.03}Sr_{0.15}Ca_{0.14}$, $^{M1}V^{3+}_{0.82}Al_{0.18}$, $^{M2}Al_{0.64}V^{3+}_{0.33}Ti^{4+}_{0.03}$, and $^{M3}Mn^{2+}_{0.71}V^{3+}_{0.26}Al_{0.02}$ for vanadoakasakaite-(La). All studied specimens are enriched in Mn^{2+}, which predominates at the $M3$ site and also occupies over 40% of the $A1$ site. The unit-cell dimensions of vanadoakasakaites are larger than those of akasakaites. This variation appears to be attributed mainly to the elongation of <$M1$-O> caused by the substitution of Al for V^{3+} at the $M1$ site. Moreover, the expansion of the $M3$ site by the substitution of divalent octahedral cations, such as Mn^{2+}, elongates the $M3$-O8 distance, which shortens the $A2$-O8 distance despite no cation substitution at the $A2$ site. This suggests that the variation in the akasakaite structure is largely influenced by cation substitution at the $M3$ and $M1$ sites. The topological change of the $A1$ polyhedra due to Mn^{2+} substitution for Ca at the $A1$ site, as reported in previous studies, was also observed.

Keywords: Akasakaite-(Ce), Akasakaite-(La), Vanadoakasakaite-(Ce), Vanadoakasakaite-(La), Epidote-supergroup, New mineral

INTRODUCTION

Epidote-supergroup minerals are found in a variety of rock types and geological settings. Among them, allanite-group minerals are an important class of rock-forming minerals that serve as reservoirs of rare earth elements (REE) (e.g., Gieré and Sorensen, 2004). The stratiform ferromanganese deposits in Japan are reported to be rich

doi:10.2465/jmps.250927
M. Nagashima, nagashim@yamaguchi-u.ac.jp Corresponding author

in REE (e.g., Kato et al., 2005; Moriyama et al., 2011; Fujinaga et al., 2011), but details of the minerals containing REE as essential components in these deposits require further study.

The general formula of epidote-supergroup minerals is represented as $A_2M_3[T_2O_7][TO_4](O, F)(OH, O)$. The A sites are subdivided into $A1$ and $A2$, while the M sites are subdivided into $M1$, $M2$, and $M3$ in the epidote structure. The volumes of the octahedral sites decrease in the order $M3 > M1 > M2$. The T sites are primarily filled with Si, although the presence of minor amounts of Al is not denied. Only a small number of species contain fluorine or lack a hydroxyl (OH) group. The structure features a single chain of edge-sharing $M2$ octahedra and a zigzag chain of central $M1$ octahedra, with $M3$ octahedra attached on alternating sides along its length. Chains of octahedra run parallel to the ***b***-axis, connected by SiO_4 and Si_2O_7 groups (Ito et al., 1954; Dollase, 1968). This structural arrangement results in 9-coordinated $A1$ and 10-coordinated $A2$ sites. In the epidote-group minerals, the $A1$ and $A2$ sites are filled with Ca, and the octahedral $M1$, $M2$, and $M3$ sites are occupied by trivalent cations. The cations with large ionic radii, such as Sr and Ba, occupy the $A2$ site, while those smaller than Ca, such as Mn^{2+}, substitute for Ca at the $A1$ site. On the other hand, the allanite-group is defined by the heterovalent substitution of the type $Ca^{2+}(A2) + Me^{3+}(M3) \leftrightarrow REE^{3+}(A2) + Me^{2+}(M3)$ (Armbruster et al., 2006). For members of the allanite-group minerals, the Levinson-type suffix designation is used to identify the dominant REE, such as La and Ce. In the epidote supergroup, the key cation sites used to define the root name are the $A1$ and M3 sites. It is recommended to use a prefix when Al is not the dominant trivalent cation at the $M1$ site (Armbruster et al., 2006).

Akasakaite-series minerals, belonging to the allanite group, are defined by the formula, ${}^{A1}Ca^{A2}REE^{3+M1}Me^{3+}{}^{M2}Al^{M3}Mn^{2+}(SiO_4)(Si_2O_7)O(OH)$. Four akasakaite-series minerals were recently discovered in the stratiform manganese deposits of Mogurazawa mine, Hishimachi, Kiryu City, Gunma Prefecture, Japan, and have been approved as new minerals: akasakaite-(Ce), akasakaite-(La), vanadoakasakaite-(Ce), and vanadoakasakaite-(La), by the Commission on New Minerals, Nomenclature and Classification (CNMNC) (IMA2025-001, 2025-002, 2024-044, and 2025-003). Type specimens are deposited in the National Museum of Nature and Science, Tokyo, Japan, with specimen numbers NSM M-53012 for akasakaite-(Ce), M-53013 for akasakaite-(La), M-52312 for vanadoakasakaite-(Ce), and M-53014 for vanadoakasakaite-(La). A reference specimen representative of the occurrence, no. 92186C is deposited in the Geological and Mineralogical Museum of Faculty of Science, Yamaguchi University. In this study, we describe the newly discovered akasakaite-series minerals and investigate their crystal-chemical properties.

OCCURRENCE AND PHYSICAL PROPERTIES

Akasakaite-(Ce), akasakaite-(La), vanadoakasakaite-(Ce), and vanadoakasakaite-(La) were found in the Mogurazawa mine, Hishimachi, Kiryu City, Gunma Prefecture, Japan (36°26′23″N 139°22′59″E). The type locality is in the Ashio Mountains district, which is mainly composed of Mesozoic Jurassic accretionary sediments. It is situated within the Kurohone-Kiryu complex in the Ashio belt, composed of greenstone, limestone, chert, and siliceous mudstone. The Kobugahara granodiorite, Sori granodiorite, and Ashikaga granodiorite are intruded in the northern, northwestern, and southern parts of the Ashio Mountains, respectively. The stratiform manganese deposits are located in sedimentary rocks, especially in chert, and the region was once home to numerous manganese mines. The Mogurazawa mine was one such manganese mine, with three known deposits: Minamiiri, Mujina, and Funegazawa (e.g., Hirowatari and Takeda, 1962). These operations continued until the 1950s. All studied materials were collected from the dumps of the Minamiiri deposit.

The primary ore minerals include rhodochrosite, rhodonite, tephroite, hausmannite, and manganosite. Occasionally, rocks are mainly composed of rhodochrosite and rhodonite, which may contain V-bearing minerals such as nagashimalite, suzukiite, and roscoelite (Matsubara and Kato, 1980; Matsubara et al., 1982). Additionally, two V-bearing minerals, zoltaiite and mannardite, were observed.

The occurrences of four akasakaite-series minerals are very similar. They occur in association with small quartz lenses within rhodonite-rich rocks and do not contact other V-containing minerals (Fig. 1). In addition, no cases of the coexistence of akasakaite-series minerals across different species have been observed to date. Since the amount of akasakaite-series minerals is very rare in this deposit, the crystals available for various measurements are also limited.

Euhedral to subhedral prismatic crystals elongated parallel to [010] are the most common form of akasakaite-(Ce), akasakaite-(La), vanadoakasakaite-(Ce), and vanadoakasakaite-(La). The crystals are dark brown with a vitreous luster, embedded in quartz (Fig. 1). The crystals range in length from a few micrometers to 1 mm. The calculated densities of akasakaite-(Ce), akasakaite-(La), vanadoakasakaite-(Ce), and vanadoakasakaite-(La) based on the empirical chemical formulae are 4.055, 4.050, 4.178, and 4.131 g/cm^3, respectively.

Figure 1. Representative occurrences of akasakaite-series minerals. Euhedral to subhedral prismatic crystals of akasakaite-(La) are dark brown with a vitreous luster.

The refractive index of vanadoakasakaite-(Ce) was measured using a liquid mixture of methylene iodide, sulfur, and tetraiodoethylene (n = 1.81). It was found that its refractive index exceeded 1.81. Since a solution with a higher refractive index was unavailable, the refractive index cannot be measured accurately directly. The mean refractive index obtained from the Gladstone-Dale relationship (Mandarino, 1981), using the empirical formula and calculated density, was 1.84, consistent with the observation (n > 1.81). On the other hand, the reflective indices of akasakaite-(Ce), akasakaite-(La), and vanadoakasakaite-(La) were not measured because of the limited number of specimens. Alternatively, the mean refractive index of each species was estimated using the Gladstone-Dale relationship (Mandarino, 1981), employing the empirical formula and calculated density: 1.81 for akasakaite-(Ce), 1.80 for akasakaite-(La), and 1.86 for vanadoakasakaite-(La). Due to a shortage of materials, other optical properties, including dispersion and pleochroism, were also not evaluated.

EXPERIMENTAL

Chemical analysis (EPMA)

Chemical analyses of the studied crystals were conducted using an electron microprobe analyzer (EPMA, JEOL JXA-8230) installed at the Centre for Instrumental Analysis, Yamaguchi University, Japan. The chemical compositions of akasakaite-(Ce), akasakaite-(La), vanadoakasakaite-(Ce), vanadoakasakaite-(La), and probe standards are listed in Table 1. Several crystals were extracted from the hand specimen and mounted individually in resin for chemical analysis of each crystal. Operating conditions were: an accelerating voltage of 15 kV, a beam current of 20 nA, and a beam diameter of 1-5 μm. Wavelength-dispersive X-ray spectra were measured using LiF, PET, and TAP monochromators to identify interfering elements and determine the optimal wavelengths for background measurements. The abundances of Si, Ti, Al, Cr, V, Fe, Mn, Co, Ni, Mg, Ca, Sr, Ba, Na, K, P, F, Cl, La, Ce, Pr, and Nd were measured. The peak and background positions of each element were carefully confirmed to avoid overlap. Several elements, which are not shown in Table 1, are below the detection limit. Although the presence of other rare-earth elements, REE, such as Y, Sm, Eu, Gd, Dy, Ho, and Er, was carefully confirmed in a preliminary analysis, they were all found to be below the detection limit. The ZAF correction method was applied to all elements. H_2O was not measured directly due to a lack of material, but the O-H stretching Raman band and single-crystal XRD refinement confirmed the presence of hydrogen. The slightly low total wt% for akasakaite-(Ce), vanadoakasakaite-(Ce), and vanadoakasakaite-(La) may be caused by electron beam damage or the effects of cracks hidden beneath the beam spot. The H_2O content in wt% was calculated based on stoichiometry.

Raman spectroscopy

Raman spectroscopy was conducted using a Renishaw inVia Reflex spectrometer equipped with a green diode laser at a wavelength of λ = 532 nm, installed at Institute for Solid State Physics, University of Tokyo, Japan. The laser power at the sample surface was approximately 10 mW. The Raman spectrum was obtained from unoriented crystals. The vanadoakasakaite-(Ce) spectrum is hardly visible due to strong photoluminescence, so it is not included. The OriginPro® 2025 software package was utilized for data analysis. The collected spectra were baseline-corrected for the continuous luminescence background. Peak positions, full widths at half maximum (FWHM), and integrated intensities were determined from fits using pseudo-Voigt functions [PV = (1 − q)*Lorentz + q*Gauss, q is the weight coefficient].

Single-crystal structure analysis

X-ray diffraction data for the single-crystal were collected using Rigaku XtaLAB Synergy-R/DW with a HyPix-6000HE diffractometer installed at Yamaguchi University, Japan. The crystals [0.05 × 0.07 × 0.15 mm for akasakaite-(Ce), 0.03 × 0.11 × 0.20 mm for akasakaite-(La), 0.02 × 0.04 × 0.06 mm for vanadoakasakaite-(Ce), and 0.21 × 0.11 × 0.07 mm for vanadoakasakaite-(La)] were mounted on a glass fiber. Intensity data were measured at room temperature using Mo$K\alpha$ radiation (λ = 0.71073 Å). Preliminary unit-cell parameters and an orientation matrix were

Table 1. Chemical compositions of akasakaite-series minerals from the Mogurazawa mine, Gunma, Japan

	Akasakaite-(Ce) IMA2025-001			Akasakaite-(La) IMA2025-002			Vanadoakasakaite-(Ce) IMA2024-044			Vanadoakasakaite-(La) IMA2025-003			Probe standard
Oxide (wt%)	Ave	Std	Range	Ave	Std	Range	Ave	Std	Range	Ave	Std	Range	
	n = 14			n = 15			n = 23			n = 21			
SiO_2	30.83	0.30	30.20-31.23	31.48	0.26	30.93-31.96	29.78	0.21	29.39-30.24	29.96	0.47	29.11-30.86	$CaSiO_3$
TiO_2	0.31	0.09	0.08-0.49	0.28	0.11	0.17-0.61	0.80	0.24	0.39-1.18	0.38	0.16	0.09-0.69	TiO_2
Al_2O_3	14.84	0.39	14.08-15.30	17.20	0.41	15.99-17.77	9.70	0.54	8.58-10.84	7.09	0.82	6.00-9.00	Al_2O_3
V_2O_3[1)]	6.39	0.53	5.78-7.33	3.84	0.20	3.48-4.23	11.49	0.34	11.03-12.13	17.44	1.47	15.33-19.63	$Ca_3(VO_4)_2$
FeO[1)]	0.23	0.04	0.17-0.29	0.14	0.08	0.00-0.31	0.28	0.06	0.16-0.44	0.01	0.02	0.00-0.07	Fe_2O_3
MnO[1)]	14.18	0.31	13.62-14.59	15.02	0.49	14.38-16.04	14.96	0.60	13.74-16.11	12.99	1.48	10.63-15.18	MnO
NiO	0.02	0.03	0.00-0.08	–			0.03	0.03	0.00-0.12	0.02	0.03	0.00-0.09	NiO
CoO	–			–			0.16	0.04	0.07-0.24	–			CoO
MgO	0.14	0.02	0.10-0.19	–			0.13	0.03	0.08-0.17	0.05	0.03	0.01-0.11	MgO
CaO	6.96	0.14	6.72-7.22	7.05	0.28	6.72-7.63	5.49	0.49	4.57-6.09	6.85	0.68	5.92-8.29	$CaSiO_3$
SrO	1.13	0.20	0.82-1.45	0.64	0.10	0.52-0.90	3.37	0.62	2.58-4.76	2.60	0.65	1.71-3.67	$SrTiO_3$
Na_2O	0.01	0.01	0.00-0.03	–			0.02	0.02	0.00-0.05	0.02	0.01	0.01-0.03	$NaAlSi_3O_8$
P_2O_5	0.01	0.01	0.00-0.04	–			0.02	0.02	0.00-0.06	0.03	0.02	0.00-0.06	$KTiOPO_4$
La_2O_3	8.12	0.27	7.71-8.46	15.12	0.75	13.72-16.57	6.19	0.53	5.36-7.06	12.06	1.43	9.77-14.01	LaB_6
Ce_2O_3	11.65	0.18	11.28-11.90	5.36	0.27	4.94-5.79	12.94	0.75	11.22-14.02	4.51	0.40	3.80-5.22	CeB_6
Pr_2O_3	0.64	0.10	0.41-0.77	0.71	0.10	0.48-0.85	0.20	0.07	0.04-0.34	0.76	0.15	0.50-1.13	PrB_6
Nd_2O_3	1.55	0.14	1.37-1.81	1.42	0.21	1.10-1.86	0.70	0.12	0.54-0.97	1.72	0.19	1.30-2.01	NdB_6
F	0.14	0.13	0.00-0.49	0.11	0.08	0.00-0.18	0.23	0.11	0.07-0.46	–			CaF_2
Cl	–			–			0.01	0.01	0.00-0.05	–			NaCl
-O=F, Cl	0.06			0.05			0.10						
Total	97.09			98.32			96.39			96.49			
H_2O (calc.)[2)]	1.48			1.51			1.38			1.49			
O = 12.5													
Si	2.99	0.01	2.98-3.04	2.99	0.02	2.95-3.02	3.00	0.01	2.95-3.02	3.01	0.02	2.98-3.03	
Ti	0.02	0.01	0.01-0.04	0.02	0.01	0.01-0.04	0.06	0.02	0.03-0.09	0.03	0.01	0.01-0.05	
Al	1.70	0.04	1.64-1.74	1.92	0.04	1.82-1.98	1.15	0.06	1.03-1.28	0.84	0.09	0.71-1.04	
V^{3+}	0.50	0.04	0.45-0.58	0.29	0.01	0.27-0.32	0.93	0.03	0.89-0.99	1.41	0.11	1.23-1.58	
Fe^{2+}	0.02	0.00	0.01-0.02	0.01	0.01	0.00-0.02	0.02	0.01	0.01-0.04	0.00	0.00	0.00-0.01	
Mn^{2+}	1.17	0.02	1.13-1.19	1.21	0.04	1.16-1.29	1.27	0.05	1.17-1.38	1.11	0.14	0.89-1.30	
Ni	0.00	0.00	0.00-0.01	–			0.00	0.00	0.00-0.01	0.00	0.00	0.00-0.01	
Co	–			–			0.01	0.00	0.01-0.02				
Mg	0.02	0.00	0.01-0.03				0.02	0.00	0.01-0.03	0.01	0.00	0.00-0.02	
Ca	0.72	0.02	0.70-0.75	0.72	0.03	0.68-0.78	0.59	0.05	0.50-0.65	0.74	0.07	0.64-0.90	
Sr	0.06	0.01	0.05-0.08	0.04	0.01	0.03-0.05	0.20	0.04	0.15-0.27	0.15	0.04	0.10-0.21	
Na	0.00	0.00	0.00-0.01	–			0.00	0.00	0.00-0.01	0.00	0.00	0.00-0.01	
P	0.00	0.00	0.00	–			0.00	0.00	0.00-0.01	0.00	0.00	0.00-0.01	
La	0.29	0.01	0.28-0.30	0.53	0.02	0.49-0.58	0.23	0.02	0.20-0.26	0.45	0.06	0.36-0.53	
Ce	0.41	0.01	0.40-0.42	0.19	0.01	0.17-0.20	0.48	0.03	0.41-0.51	0.17	0.02	0.14-0.19	
Pr	0.02	0.00	0.01-0.03	0.02	0.00	0.02-0.03	0.01	0.00	0.00-0.01	0.03	0.01	0.02-0.04	
Nd	0.05	0.00	0.05-0.06	0.05	0.01	0.04-0.06	0.03	0.00	0.02-0.03	0.06	0.01	0.05-0.07	
Total	7.97			7.98			8.00			8.01			
F^-	0.04	0.04	0.00-0.15	0.03	0.02	0.00-0.05	0.07	0.04	0.02-0.15	–			
Cl^-	–			–			0.00	0.00	0.00-0.01	–			
OH^-	0.96			0.97			0.93			1			

[1)] V, Fe, and Mn as V_2O_3, FeO, and MnO

[2)] The H_2O content was estimated based on [(OH)+F] = 1.00.

obtained from six sets of frames and refined during the integration process of the intensity data. CrysAlis^{Pro} (Agilent, 2014) was used to process the diffraction data and to correct empirical absorption. The reflection statistics and systematic absences were consistent with space groups $P2_1$ and $P2_1/m$. Subsequent attempts to solve the structure revealed that the observed average structure is centrosymmetric, indicating that $P2_1/m$ is the correct space group. Structural refinement was performed using SHELXL-2019/3 (Sheldrick, 2015). Scattering factors for neutral atoms were employed. To obtain the site-scattering values of each cation site, the site occupancies of the *A*1, *M*1, and *M*3 sites for all studied crystals were refined with Ca and Mn, Al and V, and Mn and Al scattering factors, respectively. Although the site occupancy at the *M*2 site was refined with Al and V scattering factors during the preliminary refinement, it was fixed as 1.0 Al in the final refinement if it was determined to be 1.0 Al apfu within the standard deviation. The site occupancies of the *A*2 site were refined with Ce and Ca for akasakaite-(Ce), La and Ca for akasakaite-(La) and vanadoakasakaite-(La), and Ce and Sr for vanadoakasakaite-(Ce). Moreover, the direct occupancy refinement at the *T* sites converged to full occupancy with Si scattering factors within the standard uncertainty. Then, their occupancies were fixed at 1.0 Si, which is also supported by the EPMA results. Final cation assignments were determined using the average chemical compositions of each measured crystal. Hydrogen positions of the hydroxyl groups were also derived from difference-Fourier synthesis and were refined at a fixed value of U_{iso} = 0.05Å, applying a restraint of O-H = 0.980(1) Å (Franks, 1973).

Since X-ray powder diffraction data could not be collected from all specimens due to the limited amount of material, simulated powder diffraction patterns were obtained using RIETAN-FP (Izumi and Momma, 2007) based on the results of single-crystal analyses.

RESULTS

Chemical compositions of the studied akasakaite-series minerals

The chemical compositions of the four studied akasakaite-series minerals are given in Table 1, where the cation ratios were calculated per 12.5 O atoms. The studied akasakaite-series minerals are chemically zoned, with complex elemental substitution relationships. Figure 2 shows the result of the element concentration map of vanadoakasakaite-(La) as a prime example. In all specimens, the substitution of Al ↔ V^{3+} is confirmed (Fig. 2). Moreover, the substitutions of REE^{3+} + Mn^{2+} ↔ Ca + ($Al+V^{3+}$) for akasakaite-(Ce) and -(La) and Ca ↔ Mn^{2+} and REE^{3+} + Mn^{2+} ↔ (Ca+Sr) + ($Al+V^{3+}$) for vanadoakasakaite-(Ce) and -(La) are also observed. Vanadoakasakaite-(Ce) and -(La) are enriched in Sr (~ 4.8 wt% SrO) relative to akasakaite-(Ce) and -(La) (~ 1.5 wt%). The V_2O_3 content in vanadoakasakaite-(Ce) and -(La) reaches 12.1 and 19.6 wt%, respectively. Moreover, the akasakaite-(Ce) is rich in V^{3+} (5.8-7.3 wt% V_2O_3) and poor in Al (14.1-15.3 wt% Al_2O_3) rather than the akasakaite-(La) (3.5-4.2 wt% V_2O_3 and 16.0-17.8 wt% Al_2O_3). The empirical formulae based on the average chemical data are $^{A}(Ca_{0.72}Mn^{2+}_{0.45}Ce_{0.41}La_{0.29}Nd_{0.05}Pr_{0.02}Sr_{0.06})_{\Sigma 2.00}{}^{M}(Al_{1.70}Mn^{2+}_{0.72}V^{3+}_{0.50}Mg_{0.02}Ti_{0.02}Fe_{0.02})_{\Sigma 2.98}{}^{T}(Si_{2.99}O_{11})^{O4}(O_{0.96}F_{0.04})_{\Sigma 1.00}{}^{O10}[(OH)_{0.96}O_{0.04}]_{\Sigma 1.00}$ for akasakaite-(Ce) (analytical points, n = 14), $^{A}(Ca_{0.72}Mn^{2+}_{0.45}La_{0.53}Ce_{0.19}Nd_{0.05}Pr_{0.02}Sr_{0.04})_{\Sigma 2.00}{}^{M}(Al_{1.92}Mn^{2+}_{0.76}V^{3+}_{0.29}Ti_{0.02}Fe_{0.01})_{\Sigma 3.00}{}^{T}(Si_{2.99}O_{11})^{O4}(O_{0.97}F_{0.03})_{\Sigma 1.00}{}^{O10}[(OH)_{0.97}O_{0.03}]_{\Sigma 1.00}$ for akasakaite-(La) (n = 15), $^{A}(Ca_{0.59}Mn^{2+}_{0.46}Ce_{0.48}La_{0.23}Nd_{0.03}Pr_{0.01}Sr_{0.20})_{\Sigma 2.05}{}^{M}(Al_{1.15}V^{3+}_{0.93}Mn^{2+}_{0.82}Ti^{4+}_{0.06}Fe^{2+}_{0.02}Co_{0.01}Mg_{0.02})_{\Sigma 3.01}{}^{T}(Si_3O_{11})^{O4}(O_{0.93}F_{0.07})_{\Sigma 1.00}{}^{O10}[(OH)_{0.93}O_{0.07}]_{\Sigma 1.00}$ for vanadoakasakaite-(Ce) (n = 23), and $^{A}(Ca_{0.74}Mn^{2+}_{0.40}La_{0.45}Ce_{0.17}Nd_{0.06}Pr_{0.03}Sr_{0.15})_{\Sigma 2.00}{}^{M}(V^{3+}_{1.41}Al_{0.84}Mn^{2+}_{0.71}Ti_{0.03})_{\Sigma 2.99}{}^{T}(Si_{3.01}O_{11})^{O4}O_{1.00}{}^{O10}(OH)_{1.00}$ for vanadoakasakaite-(La) (n = 21). The ideal formulae are presented as $CaCe(Al_2Mn^{2+})(Si_2O_7)(SiO_4)O(OH)$, requiring SiO_2 30.95, Al_2O_3 17.51, MnO 12.18, CaO 9.63, Ce_2O_3 28.18, H_2O 1.55, and a total of 100 wt%; $CaLa(Al_2Mn^{2+})(Si_2O_7)(SiO_4)O(OH)$, requiring SiO_2 31.02, Al_2O_3 17.54, MnO 12.21, CaO 9.65, La_2O_3 28.03, H_2O 1.55, and a total of 100 wt%; $CaCe(V^{3+}AlMn^{2+})(Si_2O_7)(SiO_4)O(OH)$, requiring SiO_2 29.73, Al_2O_3 8.41, V_2O_3 12.36, MnO

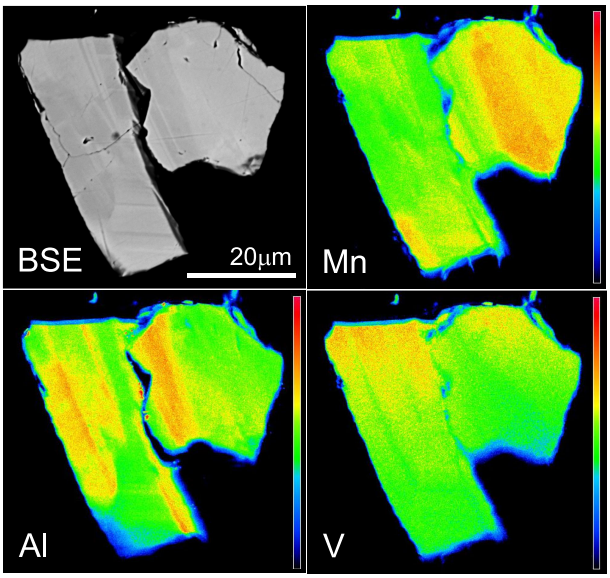

Figure 2. Back-scattered electron image and X-ray maps showing the distribution of Mn, Al, and V of vanadoakasakaite-(La).

Table 2. Data collection and details of structure refinement

		Akasakaite-(Ce) IMA2025-001	Akasakaite-(La) IMA2025-002	Vanadoakasakaite-(Ce) IMA2024-044	Vanadoakasakaite-(La) IMA2025-003
Crystal size (mm)		0.05 × 0.07 × 0.15	0.03 × 0.11 × 0.20	0.02 × 0.04 × 0.06	0.21 × 0.11 × 0.07
Space group		Monoclinic $P2_1/m$			
Unit-cell dimensions	a (Å)	8.8955(4)	8.8848(4)	8.9089(3)	8.9245(2)
	b (Å)	5.70644(19)	5.6938(2)	5.73904(17)	5.74456(12)
	c (Å)	10.1175(4)	10.0998(4)	10.1212(4)	10.1528(2)
	β (°)	113.792(5)	113.668(5)	113.616(4)	113.769(3)
	V (Å^3)	469.94(4)	467.96(4)	474.15(3)	476.36(7)
Z		2			
D_{calc} (g/cm^3)		4.055	4.050	4.178	4.131
Radiation		Mo$K\alpha$ (λ = 0.71073 Å)			
Monochromator		VariMax optics			
Diffractometer		Rigaku XtaLAB Synergy-R/DW with HyPix-6000HE			
Scan type		ω scan			
Absorption correction		CrysAlis^{Pro} (Agilent, 2014)			
Absorption coefficient μ (mm^{-1})		8.39	7.43	8.48	8.40
θ_{min}-θ_{max}(°)		2.2-40.2	2.2-40.2	2.2-40.2	2.2-40.2
Collected reflections		13143	16016	10261	16271
Unique reflections		3164	3157	3201	3221
Criterion for observed reflections					
R_{int} (%)		2.37	3.69	2.58	2.16
R_σ (%)		1.90	2.48	2.77	1.22
Index ranges		$-16 \le h \le 16$, $-10 \le k \le 10$, $-18 \le l \le 18$	$-16 \le h \le 16$, $-5 \le k \le 10$, $-18 \le l \le 17$	$-16 \le h \le 14$, $-10 \le k \le 10$, $-12 \le l \le 18$	$-16 \le h \le 16$, $-10 \le k \le 10$, $-18 \le l \le 18$
Refinement on F^2 using		SHELXL-2019/3 (Sheldrick, 2015)			
$R1$ (%)		2.32	2.86	2.23	2.20
$wR2$ (%)		6.04	7.61	5.09	5.69
No. of parameters		124	124	125	125
Weighting scheme[1)]		$w = 1/[\sigma^2(Fo^2) + (0.0170P)^2 + 0.93P]$	$w = 1/[\sigma^2(Fo^2) + (0.0368P)^2 + 0.83P]$	$w = 1/[\sigma^2(Fo^2) + (0.0188P)^2 + 0.44P]$	$w = 1/[\sigma^2(Fo^2) + (0.0203P)^2 + 0.76P]$
$\Delta\rho_{max}$ (e Å^{-3})		1.15 (0.66 Å from $A2$)	2.57 (0.66 Å from $A2$)	1.61 (0.66 Å from $A2$)	1.45 (0.60 Å from $A2$)
$\Delta\rho_{min}$ (e Å^{-3})		−0.75 (0.45 Å from Si2)	−1.88 (0.56 Å from $A2$)	−0.99 (0.55 Å from $A2$)	−0.86 (1.19 Å from O6)

[1)] The function of the weighting scheme is $w = 1/[\sigma^2(Fo^2) + (a \cdot P)^2 + b \cdot P]$, where $P = [\mathrm{Max}(Fo^2, 0) + 2Fc^2]/3$, and the parameters a and b are chosen to minimize the differences in the variances for reflections in different ranges of intensity and diffraction angle.

11.70, CaO 9.25, Ce_2O_3 27.07, H_2O 1.49, and a total of 100 wt%; and $CaLa(V^{3+}AlMn^{2+})(Si_2O_7)(SiO_4)O(OH)$, requiring SiO_2 29.79, Al_2O_3 8.43, V_2O_3 12.38, MnO 11.72, CaO 9.27, La_2O_3 26.92, H_2O 1.49, and a total of 100 wt%.

Crystal structure refinements and determination of site occupancies

Crystallographic data and refinement parameters are summarized in Table 2. The refined atomic positions are listed in Supplementary Table S1 (Supplementary Tables S1-S4 are available online from https://doi.org/10.2465/jmps.250927), and the anisotropic displacement parameters are in Table S2. Interatomic distances, selected angles, and distortions of octahedral sites are present in Table 3. The crystal structure of akasakaite-group minerals is shown in Figure 3. The simulated X-ray powder diffraction patterns from single-crystal data and the calculated patterns from the CIF file are listed in Table S3.

The number of electrons at each cation site, derived from the refined site occupancies and cation assignments for the A and M sites, is listed in Table 4. The scheme of the site occupancy determination at the $A1$, $A2$, $M1$, $M2$, and $M3$ sites is as follows: (1) Sr and REEs, such as La, Ce, Pr, and Nd, were assigned to the $A2$ site after the previous structural studies of epidote-supergroup minerals

Table 3. Selected interatomic distances (Å), bond angles (°), and distortion parameters[1)] for the octahedrally coordinated sites

		(a) Akasakaite-(Ce)	(b) Akasakaite-(La)	(c) Vanadoakasakaite-(Ce)	(d) Vanadoakasakaite-(La)
*A*1-	O1 ×2	2.348(2)	2.340(2)	2.340(1)	2.352(1)
	O3 ×2	2.266(1)	2.276(2)	2.264(1)	2.264(1)
	O5	2.535(2)	2.522(2)	2.555(2)	2.559(2)
	O7	2.289(2)	2.295(3)	2.289(2)	2.277(2)
	^{VI}<*A*1-O>	2.342	2.342	2.342	2.345
	O6	3.013(2)	2.984(2)	3.031(2)	3.054(2)
	O9 ×2	3.110(1)	3.105(1)	3.1319(7)	3.1269(8)
	^{IX}<*A*1-O>	2.587	2.583	2.594	2.597
δ[(*A*1-O6)-(*A*1-O5)]		0.478	0.462	0.476	0.495
*A*2-	O2 ×2	2.639(1)	2.651(2)	2.629(1)	2.635(1)
	O2′ ×2	2.531(1)	2.537(1)	2.536(1)	2.551(1)
	O3 ×2	2.841(2)	2.809(2)	2.869(1)	2.864(1)
	O7	2.354(2)	2.361(2)	2.369(2)	2.367(2)
	O10	2.593(2)	2.616(2)	2.594(2)	2.582(2)
	O8 ×2	2.9649(7)	2.9556(7)	2.9719(5)	2.9825(6)
	^{X}<*A*2-O>	2.690	2.688	2.697	2.701
Si1-	O1 ×2	1.646(1)	1.645(2)	1.648(1)	1.649(1)
	O7	1.590(2)	1.592(2)	1.590(2)	1.587(2)
	O9	1.631(2)	1.636(2)	1.636(2)	1.631(2)
	^{IV}<Si1-O>	1.628	1.630	1.631	1.629
O1-Si1-O1′		113.3(1)	113.1(1)	113.33(9)	113.71(9)
O1-Si1-O7		111.45(7)	111.59(7)	111.61(6)	111.58(6)
O1-Si1-O9		106.70(7)	106.81(8)	106.46(6)	106.43(6)
O7-Si1-O9		106.7(1)	106.5(1)	106.9(1)	106.6(1)
Si2-	O3 ×2	1.632(1)	1.631(1)	1.633(1)	1.632(1)
	O8	1.595(2)	1.604(2)	1.600(2)	1.595(2)
	O9	1.635(2)	1.632(2)	1.636(2)	1.636(2)
	^{IV}<Si2-O>	1.624	1.625	1.626	1.624
O3-Si2-O3′		112.4(1)	112.9(1)	112.58(8)	112.94(8)
O3-Si2-O8		110.00(7)	109.53(8)	109.95(6)	109.86(6)
O3-Si2-O9		107.49(7)	107.68(7)	107.48(6)	107.24(6)
O8-Si2-O9		109.4(1)	109.5(1)	109.3(1)	109.6(1)
Si3-	O2 ×2	1.628(1)	1.629(2)	1.626(1)	1.628(1)
	O5	1.655(2)	1.654(2)	1.658(2)	1.658(2)
	O6	1.641(2)	1.644(2)	1.641(2)	1.641(2)
	^{IV}<Si3-O>	1.638	1.639	1.638	1.639
O2-Si3-O2′		103.7(1)	103.6(1)	103.75(8)	104.02(9)
O2-Si3-O5		113.69(6)	113.61(7)	113.63(5)	113.69(5)
O2-Si3-O6		111.94(6)	111.94(7)	112.21(5)	112.02(5)
O5-Si3-O6		102.3(1)	102.5(1)	101.76(8)	101.71(9)

		(a) Akasakaite-(Ce)	(b) Akasakaite-(La)	(c) Vanadoakasakaite-(Ce)	(d) Vanadoakasakaite-(La)
*M*1-	O1 ×2	2.040(1)	2.026(2)	2.053(1)	2.060(1)
	O4 ×2	1.896(1)	1.874(1)	1.914(1)	1.926(1)
	O5 ×2	2.033(1)	2.017(1)	2.050(1)	2.054(1)
	^{VI}<M1-O>	1.990	1.972	2.006	2.013
	DI (oct)	0.031	0.033	0.030	0.029
	<λ oct>	1.004	1.005	1.003	1.003
	σ_θ (oct)^2	5.41	7.89	3.97	3.83
O1-*M*1-O4		88.34(7)	88.62(8)	88.79(6)	88.23(6)
O1-*M*1-O5		90.08(7)	90.07(7)	90.13(5)	90.15(6)
O4-*M*1-O5		93.49(6)	94.46(6)	93.07(5)	92.72(5)
*M*2-	O3 ×2	1.885(1)	1.882(1)	1.894(1)	1.913(1)
	O6 ×2	1.916(1)	1.907(1)	1.9231(9)	1.937(1)
	O10 ×2	1.902(1)	1.891(1)	1.9098(9)	1.926(1)
	^{VI}<*M*2-O>	1.901	1.893	1.909	1.925
	DI (oct)	0.006	0.005	0.005	0.004
	<λ oct>	1.005	1.006	1.005	1.004
	σ_θ (oct)^2	17.59	19.67	18.90	14.72
O3-*M*2-O6		89.46(7)	89.71(7)	89.37(6)	89.23(6)
O3-*M*2-O10		91.13(7)	91.22(7)	91.13(6)	91.18(6)
O6-*M*2-O10		96.84(5)	97.22(6)	97.09(4)	96.20(5)
*M*3-	O1 ×2	2.248(2)	2.236(2)	2.279(1)	2.276(1)
	O2 ×2	2.167(1)	2.165(2)	2.190(1)	2.171(1)
	O4	2.068(2)	2.070(2)	2.104(2)	2.075(2)
	O8	2.031(2)	2.037(3)	2.039(2)	2.034(2)
	^{VI}<*M*3-O>	2.155	2.152	2.180	2.167
	DI (oct)	0.033	0.030	0.033	0.035
	<λ oct>	1.043	1.046	1.049	1.043
	σ_θ (oct)^2	143.76	153.40	161.79	140.98
O1-*M*3-O1′		82.23(8)	82.55(9)	81.83(6)	81.89(6)
O1-*M*3-O2		90.95(5)	90.93(6)	90.83(4)	90.62(4)
O1-*M*3-O4		78.84(5)	78.47(6)	78.51(4)	79.16(4)
O1-*M*3-O8		113.14(6)	113.91(6)	114.79(4)	112.97(5)
O2-*M*3-O2′		93.13(7)	92.77(8)	93.13(6)	94.11(6)
O2-*M*3-O4		88.24(5)	88.42(6)	87.19(4)	87.82(4)
O2-*M*3-O8		80.43(6)	79.78(6)	80.21(4)	80.85(5)
O10···O4		2.886(3)	2.901(3)	2.878(3)	2.862(3)
Si1-O9-Si2		142.4(2)	142.5(2)	140.8(1)	141.9(1)

[1)] *DI*(oct) is the bond-length distortion parameter (Baur, 1974). <λ_{oct}> and σ_θ(oct)^2 are the polyhedral volume distortion and angle variance, respectively (Robinson et al., 1971).

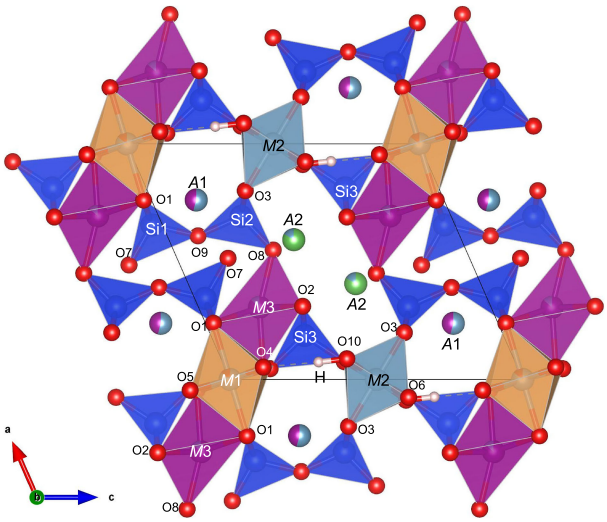

Figure 3. Crystal structure of akasakaite-series minerals using the data obtained from akasakaite-(La) projected down [010] drawn with VESTA 3 (Momma and Izumi, 2011). Dashed lines indicate H···O bonds.

(e.g., Armbruster et al., 2006), and its deficiency was filled with the Ca ions. The remaining Ca was assigned to the *A*1 site. (2) After all the remaining Ca is assigned to the *A*1 site, this site is filled with Mn^{2+}. The Mn^{2+} ions distribute in both *A*1 and *M*3 sites based on the chemical composition. (3) In many cases, the smallest *M*2 octahedral site is occupied by only Al. However, if the *M*2 site is not occupied by only Al, the cation with the next smallest ionic radius after Al is assigned. In this study, the Ti^{4+} ion is preferentially assigned to *M*2, and then the V^{3+} ion is assigned based on the observed number of electrons. (4) If the *M*2 site is occupied by only Al, the Ti^{4+} ion is assigned to the *M*1 site. In that case, the refined V occupancy at the *M*1 site is interpreted as the sum of Ti and V. The site occupancies of Al and V were determined based on the observed number of electrons calculated from the refined site occupancy value. Therefore, the occupancy refined with Al and V at the *M*1 site is directly applied to its site occupancy. (5) The remaining Mn^{2+} ions, after being assigned to *A*1, were assigned to the largest *M*3 octahedral site, due to the large ionic radius of Mn^{2+} (0.83Å after Shannon, 1976). For instance, in the case of akasakaite-(Ce), the Mn occupancy at the *M*3 site was calculated as follows: 1.17 apfu (average Mn^{2+} content determined by EPMA) − 0.45 apfu (Mn^{2+} at the A1 site) = 0.74 apfu. The

Table 4. Refined site occupancies and cation assignments with numbers of electrons of the *A* and *M* sites[1)]

Site	Refined site occupancy	Observed no. of e^-	Cation assignment	Estimated no. of e^-
(a) Akasakaite-(Ce)				
*A*1	$Ca_{0.57(1)}Mn_{0.43}$	22.15(22)	$Ca_{0.55}Mn^{2+}_{0.45}$	22.25
*A*2	$Ce_{0.764(2)}Ca_{0.236}$	49.03(10)	$(Ce_{0.41}La_{0.29}Nd_{0.05}Pr_{0.02})_{\Sigma 0.78}Sr_{0.06}Ca_{0.17}$	50.55
*M*1	$Al_{0.542(6)}V_{0.458}$	17.58(11)	$Al_{0.54}V_{0.44}Ti_{0.02}$	17.58
*M*2	$Al_{1.0}$	13	$Al_{1.0}$	13
*M*3	$Mn_{0.853(6)}Al_{0.147}$	23.24(14)	$Mn^{2+}_{0.72}Fe^{2+}_{0.02}Mg_{0.02}V^{3+}_{0.06}Al_{0.16}$	22.22
(b) Akasakaite-(La)				
*A*1	$Ca_{0.55(1)}Mn_{0.45}$	22.25(22)	$Ca_{0.54}Mn^{2+}_{0.46}$	22.30
*A*2	$La_{0.832(3)}Ca_{0.168}$	50.78(15)	$(La_{0.53}Ce_{0.18}Nd_{0.05}Pr_{0.02})_{\Sigma 0.78}Sr_{0.04}Ca_{0.18}$	49.95
*M*1	$Al_{0.853(7)}V_{0.147}$	14.47(10)	$Al_{0.85}V^{3+}_{0.13}Ti_{0.02}$	14.48
*M*2	$Al_{1.0}$	13	$Al_{1.0}$	13
*M*3	$Mn_{0.869(7)}Al_{0.131}$	23.43(16)	$Mn^{2+}_{0.75}Fe^{2+}_{0.01}V^{3+}_{0.16}Al_{0.07}$	23.60
(c) Vanadoakasakaite-(Ce)				
*A*1	$Ca_{0.588(8)}Mn_{0.412}$	22.061(8)	$Ca_{0.54}Mn^{2+}_{0.46}$	22.30
*A*2	$Ce_{0.673(4)}Sr_{0.327(4)}$	51.452(4)	$(Ce_{0.48}La_{0.23}Nd_{0.03}Pr_{0.01})_{\Sigma 0.75}Sr_{0.20}Ca_{0.05}$	51.94
*M*1	$V_{0.700(5)}Al_{0.300}$	20.000(5)	$V^{3+}_{0.70}Al_{0.30}$	20.00
*M*2	$Al_{0.831(5)}V_{0.169}$	14.691(5)	$Al_{0.83}V^{3+}_{0.11}Ti_{0.06}$	14.64
*M*3	$Mn_{0.923(5)}Al_{0.077}$	24.082(5)	$Mn^{2+}_{0.81}Fe^{2+}_{0.02}Mg_{0.02}Co_{0.01}V^{3+}_{0.12}Al_{0.02}$	24.30
(d) Vanadoakasakaite-(La)				
*A*1	$Ca_{0.565(9)}Mn_{0.435}$	22.18(20)	$Ca_{0.60}Mn_{0.40}$	22.00
*A*2	$La_{0.792(2)}Ca_{0.208}$	49.30(10)	$(La_{0.45}Ce_{0.17}Nd_{0.06}Pr_{0.03})_{\Sigma 0.71}Sr_{0.15}Ca_{0.14}$	49.38
*M*1	$V_{0.824(6)}Al_{0.176}$	21.24(13)	$V^{3+}_{0.82}Al_{0.18}$	21.20
*M*2	$Al_{0.643(6)}V_{0.357}$	16.57(10)	$Al_{0.64}V^{3+}_{0.33}Ti_{0.03}$	16.57
*M*3	$Mn_{0.895(6)}Al_{0.105}$	23.74(14)	$Mn^{2+}_{0.71}V^{3+}_{0.26}Al_{0.02}$	23.99

[1)] The chemical compositions are fixed by EPMA data.

Table 5. Bond-valence analysis (v.u.) weighted on the cation assignments of Table 4

Site	(a) Akasakaite-(Ce)	(b) Akasakaite-(La)	(c) Vanadoakasakaite-(Ce)	(d) Vanadoakasakaite-(La)
*A*1	1.95	1.95	1.91	1.95
*A*2	2.37	2.37	2.45	2.37
*M*1	2.76	2.84	2.80	2.84
*M*2	3.04	3.14	3.12	3.14
*M*3	1.91	2.06	2.09	2.06
Si1	3.97	3.96	3.94	3.96
Si2	4.01	3.99	3.99	3.99
Si3	3.86	3.86	3.86	3.86
O1	1.89	1.91	1.91	1.91
O2	1.85	1.88	1.91	1.88
O3	2.00	2.02	2.01	2.02
O4	1.53	1.58	1.57	1.58
O5	1.92	1.93	1.91	1.93
O6	2.00	2.03	2.01	2.03
O7	1.92	1.94	1.91	1.94
O8	1.70	1.71	1.76	1.71
O9	2.05	2.04	2.02	2.04
O10	1.27	1.32	1.32	1.32

6-fold coordinated divalent cations, such as Fe^{2+} and Mg, were also located at the *M*3 site for the same reason. The deficiency at *M*3 was compensated with a small amount of Al and V^{3+}.

As a result of the above scheme, the structural formulae based on 13 anions (O, OH, F) of the studied akasakaites are $^{A1}(Ca_{0.55}Mn^{2+}_{0.45})_{\Sigma1.00}{}^{A2}(Ce_{0.41}La_{0.29}Nd_{0.05}Pr_{0.02}Sr_{0.06}Ca_{0.17})_{\Sigma1.00}{}^{M1}(Al_{0.54}V^{3+}_{0.44}Ti_{0.02})_{\Sigma1.00}{}^{M2}(Al_{1.00})^{M3}(Mn^{2+}_{0.72}Fe_{0.02}Mg_{0.02}V^{3+}_{0.06}Al_{0.16})_{\Sigma0.98}Si_{2.99}O_{12}[(OH)_{0.96}F_{0.04}]_{\Sigma1.00}$ for akasakaite-(Ce), $^{A1}(Ca_{0.54}Mn^{2+}_{0.46})_{\Sigma1.00}{}^{A2}(La_{0.53}Ce_{0.18}Nd_{0.05}Pr_{0.02}Sr_{0.04}Ca_{0.18})_{\Sigma1.00}{}^{M1}(Al_{0.85}V^{3+}_{0.13}Ti_{0.02})_{\Sigma1.00}{}^{M2}Al_{1.00}{}^{M3}(Mn^{2+}_{0.75}Fe_{0.01}V^{3+}_{0.16}Al_{0.07})_{\Sigma0.99}Si_{2.99}O_{12}[(OH)_{0.97}F_{0.03}]_{\Sigma1.00}$ for akasakaite-(La), $^{A1}(Ca_{0.54}Mn^{2+}_{0.46})_{\Sigma1.00}{}^{A2}(Ce_{0.48}La_{0.23}Nd_{0.03}Pr_{0.01}Sr_{0.20}Ca_{0.05})_{\Sigma1.00}{}^{M1}(V^{3+}_{0.70}Al_{0.30})_{\Sigma1.00}{}^{M2}(Al_{0.83}V^{3+}_{0.11}Ti^{4+}_{0.06})_{\Sigma1.00}{}^{M3}(Mn^{2+}_{0.81}V^{3+}_{0.12}Fe^{2+}_{0.02}Mg_{0.02}Al_{0.02}Co_{0.01})_{\Sigma1.00}Si_{3.00}O_{12}[(OH)_{0.93}F_{0.07}]_{\Sigma1.00}$ for vanadoakasakaite-(Ce), and $^{A1}(Ca_{0.60}Mn^{2+}_{0.40})_{\Sigma1.00}{}^{A2}(La_{0.45}Ce_{0.17}Nd_{0.06}Pr_{0.03}Sr_{0.15}Ca_{0.14})_{\Sigma1.00}{}^{M1}(V^{3+}_{0.82}Al_{0.18})_{\Sigma1.00}{}^{M2}(Al_{0.64}V^{3+}_{0.33}Ti^{4+}_{0.03})_{\Sigma1.00}{}^{M3}(Mn^{2+}_{0.71}V^{3+}_{0.26}Al_{0.02})_{\Sigma0.99}Si_{3.01}O_{12}(OH)_{1.00}$ for vanadoakasakaite-(La). The dominant constituent at the *A* and *M* sites turns out to be Ca at *A*1, Ce^{3+} or La^{3+} at *A*2, Al or V^{3+} at *M*1, Al at *M*2, and Mn^{2+} at *M*3.

Bond-valence sums were calculated using the electrostatic strength function of Brown and Altermatt (1985) and the bond-valence parameters of Gagné and Hawthorne (2015). The results are given in Table 5. The calculated bond-valence sums and refined hydrogen positions indicate that one hydroxyl group is located at O10 (donor, 1.27-1.32 valence unit, v.u.) with O4 acting as acceptor (1.53-1.58 v.u.). The valence unit of O8 (1.70-1.76 v.u.) is smaller than the expected 2 v.u. of O, which is due to the elongation of the *M*3-O8 and *A*2-O8 bonds, which will be discussed later.

Raman spectra of akasakaite-series minerals

Figure 4 shows the spectra of four akasakaites in the ranges 115-1250 (lattice vibration region) and 2650-3820 (OH region) cm^{-1} with the spectra of allanite-(La), RRUFF R070246 (unoriented with 532 nm laser, Lafuente et al., 2015) and allanite-(Ce), RRUFF080044 (unoriented with 532 nm laser, heated at 850 °C for 18 h) as references. The peak around 570 cm^{-1} is assigned to the Si-O_b-Si bending mode of the monoclinic epidote structure, as reported by Nagashima and Mihailova (2023). Although the peak around 693 cm^{-1} is generally not observed in Al-Fe^{3+} series epidote, it is typically observed in allanite-group minerals. In the O-H stretching region, several peaks centered at approximately 3250 cm^{-1} overlap, which appears to be due to the different local chemical surroundings of the acceptor oxygen anion.

DISCUSSION

Structural variations related to the cation substitution

In allanite-group minerals, the *M*3 site is occupied by the octahedral divalent cations (= Me^{2+}) to balance the REE^{3+} in the *A*2 site. The expansion of *M*3 octahedra is significant because of the large ionic radii of Me^{2+}, such as Fe^{2+},

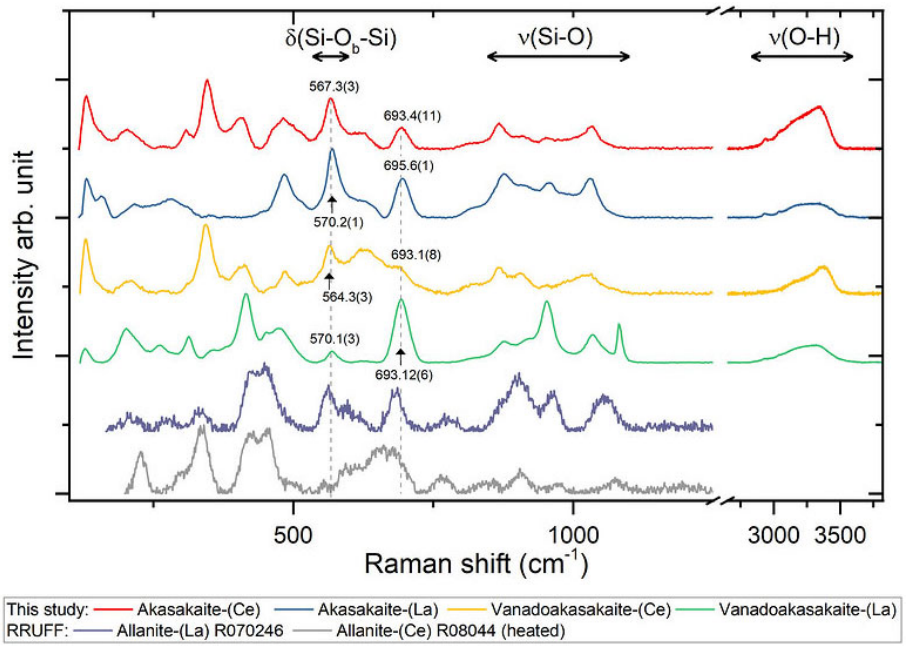

Figure 4. Raman spectra of the studied akasakaites in the ranges 115–1250 (lattice vibration region) and 2600–3800 (OH region) cm^{-1} with the spectra of allanite-(La), RRUFF R070246, and allanite-(Ce), RRUFF080044 (unoriented with 532 nm laser, heated at 850 °C for 18 h) as reference.

Mn^{2+}, and Mg. Among the Me^{2+} ions primarily located in the *M*3 site of the epidote structure, the Mn^{2+} ion is the largest octahedral divalent cation (0.83 Å, 6-coordinated; Shannon, 1976). Hence, the akasakaite- and androsite-series minerals, where Mn^{2+} dominates at the *M*3 site, exhibit a long <*M*3-O> distance. In this study, 81% of the *M*3 site in vanadoakasakaite-(Ce) is occupied by Mn^{2+}, and the <*M*3-O> distance attains 2.180 Å (Tables 4 and 5). Moreover, among the studied akasakaites, vanadoakasakaite-(Ce) and -(La) have elongated <*M*1-O> due to the predominant V^{3+} ions in the *M*1 sites, with <*M*1-O> reaching 2.006 and 2.013 Å, respectively, while akasakaite-(Ce) and -(La) have <*M*1-O> = 1.990 and 1.972 Å, respectively (Table 3).

Divalent octahedral cation substitution for Al at the *M*3 site significantly increases the *M*3-O8 distance, causing the O8 site to shift away from the *M*3 cation. Since the O atom at the O8 site is shared with the *A*2, *M*3, and Si2 sites (Fig. 3), this shift of O8 caused by the expansion of the *M*3 site results in the shortened *A*2-O8 distance (Fig. 5). The *A*2-O*i* distance is primarily influenced by the cation distribution in the *A*2 site, as exemplified in a study of synthetic Sr-bearing clinozoisites (Dörsam et al., 2007). However, even if the *A*2 site is completely occupied by Ca and no substitution has taken place, the *A*2-O8 distance decreases with the increase of the *M*3-O8 distance (e.g., summarized data for the Al-Fe^{3+} series by Franz and Liebscher, 2004). Figure 5 shows the relationship between the *M*3-O8 and *A*2-O8 distances in allanite-group minerals. In the androsites (Mn^{2+} at the *A*1 and *M*3 sites), the *A*2-O8 distance is short, despite the predominance of

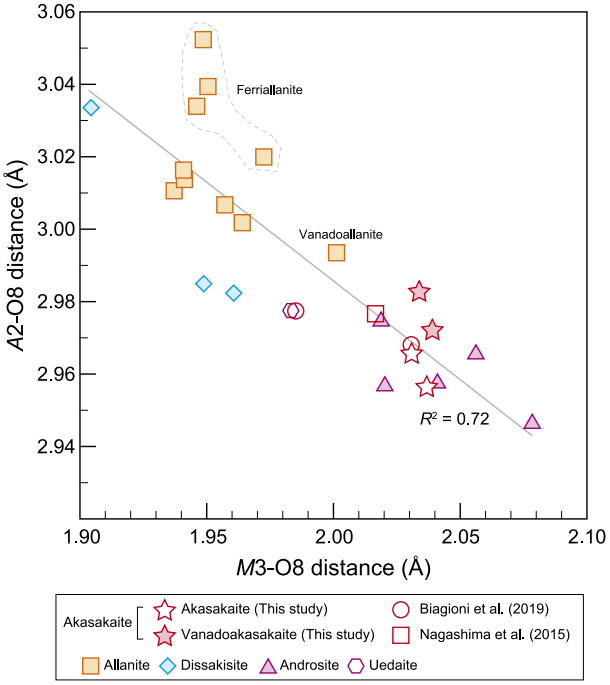

Figure 5. Relationship between the *M*3-O8 and *A*2-O8 distances. Data for the allanite group listed in Table S4 are plotted. Standard deviations (1σ) are smaller than the symbol size. Data sources are as follows: This study, Dollase (1971), Rouse and Peacor (1993), Bonazzi et al. (1996), Kartashov et al. (2002), Hoshino et al. (2005), Cenki-Tok et al. (2006), Lavina et al. (2006), Orlandi and Pasero (2006), Hoshino et al. (2008), Miyawaki et al. (2008), Hoshino et al. (2010), Nagashima et al. (2011), Kolitsch et al. (2012), Škoda et al. (2012), Nagashima et al. (2013, 2015), Biagioni et al. (2019), and Števko et al. (2023).

REE^{3+} at the *A*2 site, as well as in the other allanites (Fig. 5 and Table S4). The shortened *A*2-O8 distance results from the elongation of *M*3-O8 caused by the substitution of Mn^{2+} at the *M*3 site. Furthermore, the *A*2-O8 distance of the $^{M1}Me^{3+}$-dominant species, such as ferriallanite and vanadoallanite, as well as the vanadoakasakaite in this study, is generally longer than expected (Fig. 5), which is attributed to the expansion of the *M*1 site. Therefore, it is evident that the cation distribution of the *M*3 and *M*1 sites substantially influences not only the octahedral sites but also the adjacent coordination polyhedra and, ultimately, the entire epidote structure.

Moreover, the substitution of Mn^{2+} for Ca at *A*1 causes the topological change of 9-coordinated *A*1 polyhedra (Bonazzi et al., 1996; Nagashima et al., 2010, 2013, 2015; Biagioni et al., 2019). According to previous studies, as Mn^{2+} increases at the *A*1 site, the oxygen atoms at the O3 and O1 sites (2^{nd} to 5^{th} neighbor O atoms) move closer to *A*1, while O6 (7^{th} neighbor) and O9 (8^{th} and 9^{th} neighbors) shift away from *A*1. In contrast, since the positions of O5 (6^{th} neighbor) remain unaffected, the lengthened δ[(*A*1-O6)-(*A*1-O5)] distance (Å) seems to be a good indicator of Mn^{2+} at the *A*1 site. In this study, the large δ value has also been confirmed (Fig. 6), ranging from 0.462 Å (against $Ca_{0.54}Mn^{2+}_{0.46}$ at *A*1) in akasakaite-(La) to 0.495 Å (against $Ca_{0.60}Mn^{2+}_{0.40}$ at *A*1) in vanadoakasakaite-(La) (Table 3).

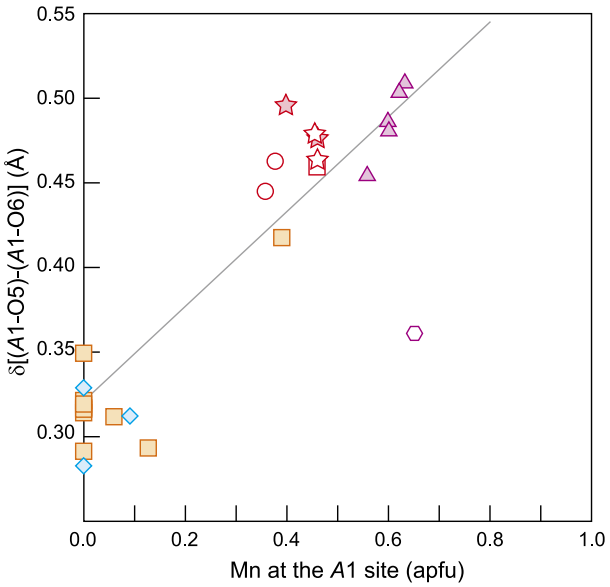

Figure 6. The variation of δ[(*A*1-O5)-(*A*1-O6)] (Å) as a function of Mn^{2+} content at the *A*1 site. The solid line is the regression line suggested by Biagioni et al. (2019): δ[(*A*1-O5)-(*A*1-O6)] (Å) = 0.32(1) + 0.28 × Mn^{2+} at *A*1 (apfu). Data for allanite-group listed in Table S4 are plotted. The symbols are the same as in Figure 5.

Effect of cation behavior on the unit cell parameters, particularly on the *β* angle

Based on the systematic studies of the synthetic Ca-analogue clinozoisite-group minerals, cation distributions at the *M*3 and *M*1 sites strongly influence the *a*-, *b*-, and *c*-dimensions, whereas little influence on the variation in the *β* angle (e.g., Anastasiou and Langer, 1977; Giuli et al., 1999; Langer et al., 2002; Nagashima and Akasaka, 2004; Nagashima et al., 2009; Nagashima and Akasaka, 2010). On the other hand, the results of the structural analysis of synthetic Sr-bearing clinozoisite, reported by Dörsam et al. (2007), indicated that a systematic decrease of the *β* angle with increasing Sr content at the *A*2 site (115.42° with $Sr_{0.128}Ca_{0.872}$ at *A*2 and 114.99° with $Sr_{0.878}Ca_{0.122}$ at *A*2). It was interpreted as resulting from the compression of the *M*3 and Si3 polyhedra, and the expansion of the *A*2 polyhedron. It is also well established that in REE-bearing epidote group minerals, REE^{3+} at the *A*2 site and Me^{2+} at the octahedral sites lead to an expansion of the unit-cell dimensions, while the *β* angle decreases with increasing REE content at the *A*2 site (Bonazzi and Menchetti, 1994, 1995; Bonazzi et al., 1996; Bonazzi and Menchetti, 2004; Gieré and Sorensen, 2004). Furthermore, the *β* angle of REE-bearing epidote-supergroup minerals with Mn^{2+} at *A*1 is generally smaller than that of those without Mn^{2+} at *A*1 (Nagashima et al., 2015). This smaller *β* angle is typically observed in the androsite series, in the range of 113.09-113.90° (Table S4, Bonazzi et al., 1996; Cenki-Tok et al., 2006; Nagashima et al., 2015; Števko et al., 2023). In the akasakaite-series minerals, the predominant cation at the *A*1 site is Ca; however, in many cases, part of the *A*1 site is occupied by Mn^{2+}, which often results in the small *β* angle (113.62°-113.77° in Table 2), similar to that of androsite (Nagashima et al., 2015; Biagioni et al., 2019). Therefore, this study also confirmed that the *β* angle varies depending on the Mn^{2+} content of the *A*1 site, as well as the REE and Sr contents of the *A*2 site. It is supported by the roughly negative correlation between the *β* angle and the Mn + REE + Sr content at the *A*1 and *A*2 sites (Fig. 7). Nevertheless, since the *β* angle of uedaite (114.52° from SXRD, and 115.10° from PXRD) examined by Miyawaki et al. (2008) tends to be larger than expected (Fig. 7), we must consider the possibility that the interplay of dominant cation species at the *M*1 and *M*3 sites, alongside the *A*1 and *A*2 sites, produces a complex effect that warrants further investigation.

Nomenclature and relationship to other species

The four species studied here belong to the epidote-supergroup mineral, which is classified as 58.2 in the Dana clas-

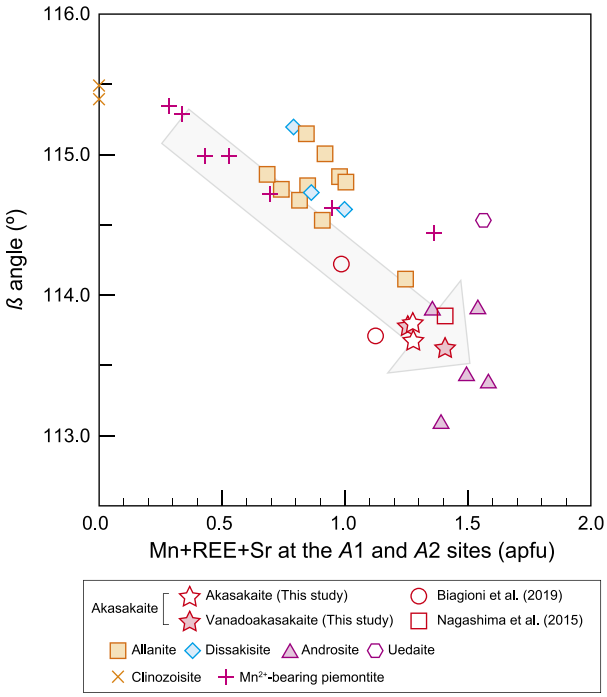

Figure 7. Variation of the β-angle as a function of Mn^{2+} + REE^{3+} + Sr at the $A1$ and $A2$ sites. Data listed in Table S4 are plotted. Data sources not represented in the caption of Figure 5 are as follows: Bonazzi et al. (1990, 1992, 1996), Comodi and Zanazzi (1997), Dollase (1968), and Nagashima et al. (2010). Standard deviations (1σ) are smaller than the symbol size.

sification and 09.BG.05b in the Nickel-Strunz classification. They were named in accordance with the recommended nomenclature of epidote-supergroup minerals (Armbruster et al., 2006). The root name, akasakaite, $^{A1}Ca^{A2}REE^{3+M1}Al^{M2}Al^{M3}Mn^{2+}(Si_2O_7)(SiO_4)O(OH)$, is applied for minerals in which Ca and Mn^{2+} are the dominant cations at the $A1$ and $M3$ sites, respectively. A prefix should be added if the dominant cation at the $M1$ site is not aluminum, and the predominant REE cation at the $A2$ site should be noted as an extended Levison suffix. The ideal formulae of each specimen were represented as $^{A1}Ca^{A2}Ce^{M1}Al^{M2}Al^{M3}Mn^{2+}(Si_2O_7)(SiO_4)O(OH)$, $^{A1}Ca^{A2}La^{M1}Al^{M2}Al^{M3}Mn^{2+}(Si_2O_7)(SiO_4)O(OH)$, $^{A1}Ca^{A2}Ce^{M1}V^{3+M2}Al^{M3}Mn^{2+}(Si_2O_7)(SiO_4)O(OH)$, and $^{A1}Ca^{A2}La^{M1}V^{3+M2}Al^{M3}Mn^{2+}(Si_2O_7)(SiO_4)O(OH)$, and they named akasakaite-(Ce) (IMA2025-001), akasakaite-(La) (IMA2025-002), vanadoakasakaite-(Ce) (IMA2024-044) and vanadoakasakaite-(La) (IMA2025-003), respectively. The former two and the latter two species are related by the homovalent substitution of Al ↔ V^{3+} at the $M1$ site. They are also related to the ferriakasakaite-(La), ferriakasakaite-(Ce), manganiakasakaite-(La), which are known as species belonging to the akasakaite series (Nagashima et al., 2015; Biagioni et al., 2019). The Mn^{2+}-enriched akasakaite-series minerals are closely related to androsite-series, represented as $^{A1}Mn^{2+A2}REE^{3+M1}(Mn^{3+}, Fe^{3+}, V^{3+})^{M2}Al^{M3}Mn^{2+}(Si_2O_7)(SiO_4)O(OH)$ (Bonazzi et al., 1996; Cenki-Tok et al., 2006; Nagashima et al., 2015; Števko et al., 2023). Androsite-akasakaite solid solution commonly occurs, characterized by the Ca ↔ Mn^{2+} substitution at the A1 site (e.g., Bonazzi et al., 1996; Cenki-Tok et al., 2006; Nagashima et al., 2015).

ACKNOWLEDGMENTS

We thank Mr. Yoji Morifuku (Center for Instrumental Analysis, Yamaguchi University) for his technical assistance. We also thank the editor, Dr. M. Hamada, and two anonymous reviewers for their comments. This study results from the utilization of research equipment shared in the MEXT Project for Promoting Public Utilization of Advanced Research Infrastructure (Program for supporting the construction of core facilities), Grant Nos. JPMXS0440400023 and JPMXS0440400024, and it is also supported by the Core Clusters for Research Initiative of Yamaguchi University. One of the authors, M.N., gratefully acknowledges the financial support of Grants-in-Aid for Scientific Research from the Japan Society for the Promotion of Science, No. JP23K03551.

SUPPLEMENTARY MATERIALS

Supplementary Tables S1-S4 and CIF files are available online from https://doi.org/10.2465/jmps.250927.

REFERENCES

Agilent (2014) CrysAlis PRO. Agilent Technologies Ltd., Yarnton, Oxfordshire, England.

Anastasiou, P. and Langer, K. (1977) Synthesis and physical properties of piemontite $Ca_2Al_{3-p}Mn_p^{3+}(Si_2O_7/SiO_4/O/OH)$. Contributions to Mineralogy and Petrology, 60, 225-245.

Armbruster, T., Bonazzi, P., Akasaka, M., Bermanec, V., et al. (2006) Recommended nomenclature of epidote-group minerals. European Journal of Mineralogy, 18, 551-567.

Baur, H. (1974) The geometry of polyhedral distortions. Predictive relationships for the phosphate group. Acta Crystallographica, B30, 1195-1215.

Biagioni, C., Bonazzi, P., Pasero, M., Zaccarini, F., et al. (2019) Manganiakasakaite-(La) and ferriakasakaite-(Ce), two new epidote supergroup minerals from Piedmont, Italy. Minerals, 9, 353.

Bonazzi, P., Menchetti, S. and Palenzona, A. (1990) Strontiopiemontite, a new member of the epidote group, from Val Graveglia, Liguria, Italy. European Journal of Mineralogy, 2, 519-523.

Bonazzi, P., Garbarino, C. and Menchetti, S. (1992) Crystal chemistry of piemontites; REE-bearing piemontite from Monte Brugiana, Alpi Apuane, Italy. European Journal of Mineralogy, 4, 23-33.

Bonazzi, P. and Menchetti, S. (1994) Structural variations induced

by heat treatment in allanite and REE-bearing piemontite. American Mineralogist, 79, 1176-1184.

Bonazzi, P. and Menchetti, S. (1995) Monoclinic members of the epidote group: effects of the Al ↔ Fe^{3+} ↔ Fe^{2+} substitution and of the entry of REE^{3+}. Mineralogy and Petrology, 53, 133-153.

Bonazzi, P., Menchetti, S. and Reinecke, T. (1996) Solid solution between piemontite and androsite-(La), a new mineral of the epidote group from Andros Island, Greece. American Mineralogist, 81, 735-742.

Bonazzi, P. and Menchetti, S. (2004) Manganese in monoclinic members of the epidote group: piemontite and related minerals. In Reviews in Mineralogy and Geochemistry, Vol. 56 Epidotes, Mineralogical Society of America, Washington, 495-552. https://doi.org/10.2138/gsrmg.56.1.495

Brown, I.D. and Altermatt, D. (1985) Bond-valence parameters obtained from a systematic analysis of the inorganic crystal structure database. Acta Crystallographica, B41, 244-247.

Cenki-Tok, B., Ragu, A., Armbruster, T., Chopin, S. and Medenbach, O. (2006) New Mn- and rare-earth-rich epidote-group minerals in metacherts: manganiandrosite-(Ce) and vanadoandrosite-(Ce). European Journal of Mineralogy, 18, 569-582.

Comodi, P. and Zanazzi, P.F. (1997) The pressure behavior of clinozoisite and zoisite: An X-ray diffraction study. American Mineralogist, 82, 61-68.

Dollase, W.A. (1968) Refinement and comparison of the structures of zoisite and clinozoisite. American Mineralogist, 53, 1882-1898.

Dollase, W.A. (1971) Refinement of the crystal structures of epidote, allanite and hancockite. American Mineralogist, 56, 447-464.

Dörsam, G., Liebscher, A., Wunder, B., Franz, G. and Gottschalk, M. (2007) Crystal chemistry of synthetic $Ca_2Al_3Si_3O_{12}OH$-$Sr_2Al_3Si_3O_{12}OH$ solid-solution series of zoisite and clinozoisite. American Mineralogist, 92, 1133-1147.

Franks, F., Ed. (1973) Water: A comprehensive treatise, vol. 2, pp. 684, Plenum, New York.

Franz, G. and Liebscher, A. (2004) Physical and chemical properties of the epidote minerals-An introduction-. In Epidotes (Liebscher, A. and Franz, G. Eds.). Reviews in Mineralogy and Geochemistry, Vol. 56, Mineralogical Society of America, Geochemical Society, 1-82. https://doi.org/10.2138/gsrmg.56.1.1

Fujinaga, K., Nozaki, T., Nakayama, K. and Kato, Y. (2011) Rare earth resource potential of the Aki strata-bound Fe-Mn deposit in the Northern Shimanto Belt, central Shikoku, Japan. Shigen-Chishitsu, 61, 1-11 (Japanese with English abstract).

Gagné, O.C. and Hawthorne, F.C. (2015) Comprehensive derivation of bond-valence parameters for ion pairs involving oxygen. Acta Crystallographica, B71, 562-578.

Gieré, R. and Sorensen, S.S. (2004) Allanite and other REE-rich epidote-group minerals. In Reviews in Mineralogy and Geochemistry, Vol. 56 Epidotes, Mineralogical Society of America, Washington, 431-493. https://doi.org/10.2138/gsrmg.56.1.431

Giuli, G., Bonazzi, P. and Menchetti, S. (1999) Al-Fe disorder in synthetic epidotes: A single-crystal X-ray diffraction study. American Mineralogist, 84, 933-936.

Hirowatari, F. and Takeda, H. (1962) On the manganese ore deposits in the Kaso, Hikoma and Hishimura districts, Tochigi Prefecture -report of the manganese silicate deposits in Japan (5)-. Bulletin of the Geological Survey of Japan, 13, 683-708 (in Japanese with English abstract).

Hoshino, M., Kimata, M., Nishida, N., Kyono, A., et al. (2005) The chemistry of allanite from the Daibosatsu Pass, Yamanashi, Japan. Mineralogical Magazine, 69, 403-423.

Hoshino, M., Kimata, M., Nishida, N. and Shimizu, M. (2008) Crystal chemical significance of chemical zoning in dissakisite-(Ce). Physics and Chemistry of Minerals, 35, 59-70.

Hoshino, M., Kimata, M., Chesner, C.A., Nishida, N., et al. (2010) Crystal chemistry of volcanic allanites indicative of naturally induced oxidation-dehydrogenation. Mineralogy and Petrology, 99, 133-141.

Ito, T., Morimoto, N. and Sadanaga, R. (1954) On the structure of epidote. Acta Crystallographica, 7, 53-59.

Izumi, F. and Momma, K. (2007) Three-dimensional visualization in powder diffraction. Solid State Phenomena, 130, 15-20.

Kartashov, P.M., Ferraris, G., Ivaldi, G., Sokolova, E. and McCammon, C.A. (2002) Ferriallanite-(Ce), $CaCeFe^{3+}AlFe^{2+}(SiO_4)(Si_2O_7)O(OH)$, a new member of the epidote group: description, X-ray and Mössbauer study. The Canadian Mineralogist, 40, 1641-1648.

Kato, Y., Fujinaga, K., Nozaki, T., Osawa, H., et al. (2005) Rare earth, major and trace elements in the Kunimiyama ferromanganese deposit in the Northern Chichibu belt, Central Shikoku, Japan. Resource Geology, 55, 291-300.

Kolitsch, U., Mills, S.J., Miyawaki, R. and Blass, G. (2012) Ferriallanite-(La), a new member of the epidote supergroup from the Eifel, Germany. European Journal of Mineralogy, 24, 741-747.

Lafuente, B., Downs, R.T., Yang, H. and Stone, N. (2015) The power of databases: the RRUFF project. In Highlights in Mineralogical Crystallography (Armbruster, T. and Danisi, R.M. Eds.). W. De Gruyter, Berlin, Germany, 1-30. https://doi.org/10.1515/9783110417104-003

Langer, K., Tillmanns, E., Kersten, M., Almen, H. and Arni, R.K. (2002) The crystal chemistry of Mn^{3+} in the clino- and orthozoisite structure types, $Ca_2M^{3+}_3[OH/O/SiO_4/Si_2O_7]$: A structural and spectroscopic study of some natural piemontites and "thulites" and their synthetic equivalents. Zeitschrift für Kristallographie, 217, 563-580.

Lavina, B., Carbonin, S., Russo, U. and Tumiati, S. (2006) The crystal structure of dissakisite-(La) and structural variations after annealing of radiation damage. American Mineralogist, 91, 104-110.

Mandarino, J.A. (1981) The Gladstone-Dale relationship: Part IV. The compatibility concept and its application. The Canadian Mineralogist, 19, 441-450.

Matsubara, S. and Kato, A. (1980) Nagashimalite, $Ba_4(V^{3+},Ti)_4[(O,OH)_2|Cl|Si_8B_2O_{27}]$, a new mineral from the Mogurazawa mine, Gumma prefecture, Japan. Mineralogical Journal, 10, 122-130.

Matsubara, S., Kato, A. and Yui, S. (1982) Suzukiite, $Ba_2V^{4+}_2[O_2|Si_4O_{12}]$, a new mineral from the Mogurazawa mine, Gumma Prefecture, Japan. Mineralogical Journal, 11, 15-20.

Miyawaki, R., Yokoyama, K., Matsubara, S., Tsutsumi, Y. and Goto, A. (2008) Uedaite-(Ce), a new member of the epidote group with Mn at the A site, from Shodoshima, Kagawa Prefecture, Japan. European Journal of Mineralogy, 20, 261-269.

Momma, K. and Izumi, F. (2011) VESTA3 for three-dimensional visualization of crystal, volumetric and morphology data. Journal of Applied Crystallography, 44, 1272-1276.

Moriyama, T., Miyawaki, R., Yokoyama, K., Matsubara, S., et al. (2011) Wakefieldite-(Nd), a new neodymium vanadate mineral in the Arase Stratiform ferromanganese deposit, Kochi Prefecture, Japan. Resource Geology, 61, 101-110.

Nagashima, M. and Akasaka, M. (2004) An X-ray Rietveld study of piemontite on the join $Ca_2Al_3Si_3O_{12}(OH)$ - $Ca_2Mn^{3+}_3Si_3O_{12}(OH)$ formed by hydrothermal synthesis. American Mineralo-

gist, 89, 1119-1129.

Nagashima, M., Geiger, C.A. and Akasaka, M. (2009) A crystal-chemical investigation of clinozoisite synthesized along the join $Ca_2Al_3Si_3O_{12}(OH)$-$Ca_2Al_2CrSi_3O_{12}(OH)$. American Mineralogist, 94, 1351-1360.

Nagashima, M. and Akasaka, M. (2010) X-ray Rietveld and ^{57}Fe Mössbauer studies of epidote and piemontite on the join $Ca_2Al_2Fe^{3+}Si_3O_{12}(OH)$ - $Ca_2Al_2Mn^{3+}Si_3O_{12}(OH)$ formed by hydrothermal synthesis. American Mineralogist, 95, 1237-1246.

Nagashima, M., Armbruster, T., Akasaka, M. and Minakawa, T. (2010) Crystal chemistry of Mn^{2+}-, Sr-rich and REE-bearing piemontite from the Kamisugai mine in the Sambagawa metamorphic belt, Shikoku, Japan. Journal of Mineralogical and Petrological Sciences, 105, 142-150.

Nagashima, M., Imaoka, T. and Nakashima, K. (2011) Crystal chemistry of Ti-rich ferriallanite-(Ce) from Cape Ashizuri, Shikoku Island, Japan. American Mineralogist, 96, 1870-1877.

Nagashima, M., Nishio-Hamane, D., Tomita, N., Minakawa, T. and Inaba, S. (2013) Vanadoallanite-(La): a new epidote-supergroup mineral from Ise, Mie Prefecture, Japan. Mineralogical Magazine, 77, 2739-2752.

Nagashima, M., Nishio-Hamane, D., Tomita, N., Minakawa, T. and Inaba, S. (2015) Ferriakasakaite-(La) and ferriandrosite-(La): new epidote-supergroup minerals from Ise, Mie Prefecture, Japan. Mineralogical Magazine, 79, 735-753.

Nagashima, M. and Mihailova, B. (2023) Optimal Raman-scattering signal for estimating the Fe content on the clinozoisite-epidote join. European Journal of Mineralogy, 35, 267-283.

Orlandi, P. and Pasero, M. (2006) Allanite-(La) from Buca della Vena mine, Apuan Alps, Italy, an epidote-group mineral. The Canadian Mineralogist, 44, 63-68.

Robinson, K., Gibbs, G.V. and Ribbe, P.H. (1971) Quadratic elongation: a quantitative measure of distortion in coordination polyhedra. Science, 172, 567-570.

Rouse, R.C. and Peacor, D.R. (1993) The crystal structure of dissakisite-(Ce), the Mg analogue of allanite-(Ce). The Canadian Mineralogist, 31, 153-157.

Shannon, R.D. (1976) Revised effective ionic radii and systematic studies of interatomic distances in halides and chalcogenides. Acta Crystallographica, A32, 751-767.

Sheldrick, G.M. (2015) Crystal structure refinement with SHELX. Acta Crystallographica, C71, 3-8.

Škoda, R., Cempírek, J., Filip, J., Novák, M., et al. (2012) Allanite-(Nd), $CaNdAl_2Fe^{2+}(SiO_4)(Si_2O_7)O(OH)$, a new mineral from Åskagen, Sweden. American Mineralogist, 97, 983-988.

Števko, M., Myšľan, P., Biagioni, C., Mauro, D. and Mikuš, T. (2023) Ferriandrosite-(Ce), a new member of the epidote supergroup from Betliar, Slovakia. Mineralogical Magazine, 87, 887-895.

Manuscript received September 27, 2025
Manuscript accepted December 17, 2025
Advance online publication December 26, 2025
Released online publication January 23, 2026
Manuscript handled by Maki Hamada